

Bipartite Solution to the Lithium Problem

Sougata Ganguly^{1,*}, Tae Hyun Jung^{1,†}, Tae-Sun Park^{2,‡} and Chang Sub Shin^{3,1,4,§}

¹*Particle Theory and Cosmology Group (PTC), Center for Theoretical Physics of the Universe (CTPU),
Institute for Basic Science, Daejeon 34126, Republic of Korea*

²*Center for Exotic Nuclear Studies (CENS),
Institute for Basic Science, Daejeon 34126, Republic of Korea*

³*Department of Physics and Institute for Sciences of the Universe,
Chungnam National University, Daejeon 34134, Republic of Korea*

⁴*Korea Institute for Advanced Study, Seoul 02455, South Korea*

The primordial lithium problem remains a persistent motivation for new-physics modifications of Big Bang nucleosynthesis, yet the precision of the observed deuterium abundance now places strong constraints on such attempts. This indicates that the challenge is not simply to reduce ${}^7\text{Li}$, but to realize the correlated shifts among light-element abundances required to do so without spoiling deuterium. We investigate this issue in a concrete two-step decay scenario involving two unstable particles undergoing sequential late decays. In the first stage, a majoron with lifetime $\tau_J \sim 10 - 10^4$ sec decays predominantly into neutrinos, increasing the neutron abundance and thereby reducing the primordial ${}^7\text{Li} + {}^7\text{Be}$ yield. This mechanism, however, simultaneously drives deuterium above the observationally allowed range. In the second stage, an axion-like particle with a longer lifetime $\tau_\phi \gtrsim 10^5$ sec decays into photons, inducing late-time photodissociation that compensates the excess deuterium without erasing the earlier reduction of lithium, while further amplifying the depletion of ${}^7\text{Li} + {}^7\text{Be}$. Although the setup is model-dependent, it serves as an explicit proof of concept that the lithium abundance can be lowered consistently with current deuterium constraints. More broadly, our analysis highlights that a viable resolution may require a nontrivial combination of decay channels and decay epochs, and clarifies the pattern of abundance response that successful late-decay scenarios must achieve.

I. INTRODUCTION

The discrepancy in ${}^7\text{Li}$ abundance between the predicted value of Big Bang nucleosynthesis (BBN) [1] and the observed value based on the so-called Spite plateau [2] has been a long-standing puzzle, known as the lithium problem. The standard BBN (SBBN) predicts $({}^7\text{Li}/\text{H})_{\text{SBBN}} = (5.464 \pm 0.220) \times 10^{-10}$ [3, 4] (see also Refs. [5–8] where theoretically predicted numbers are consistent with a small difference) which is almost three times higher than its observed value $({}^7\text{Li}/\text{H})_{\text{obs}} = (1.45 \pm 0.25) \times 10^{-10}$ [9, 10] (roughly 4σ deviation). Since the main nuclear reactions in SBBN are well measured and the baryon density is fixed by the CMB, this tension suggests that there may be either some new astrophysical effects or physics beyond the Standard Model (BSM).

One possible solution is that the primordial ${}^7\text{Li}$ has been depleted during stellar evolution, so the observed abundance today may be lower than the original value. If the depletion is large enough, the lithium problem can be solved. This idea, often called the stellar depletion scenario, has been studied in many works (see, for example, Refs. [11–31]). Although the idea is simple and plausible, reproducing the flat Spite plateau and its small dispersion over a wide range of metallicity and temperature has been challenging. Various macroscopic flows

involving different physics turned out to be important, and some models incorporating them could successfully reproduce the Spite plateau [32]. Moreover, the recent non-observation of ${}^6\text{Li}$ in three Spite plateau stars [33] indicates a large depletion of ${}^6\text{Li}$, supporting the stellar depletion of ${}^7\text{Li}$ [34]. Nevertheless, there are still model parameters that lack derivation from the first principles, and thus we still need an explanation of why these model parameters should be specific values that solve the ${}^7\text{Li}$ problem.

Alternatively, the primordial ${}^7\text{Li}$ abundance may have been reduced by BSM effects, which we focus on in this work. In SBBN, most of the final ${}^7\text{Li}$ comes from ${}^7\text{Be}$ that later decays into ${}^7\text{Li}$ after BBN. Thus, the lithium problem indicates that the ${}^7\text{Be}$ abundance from SBBN is too large, and various BSM scenarios have been proposed to reduce it [35–51].

However, the difficulty lies in maintaining the prediction for the primordial abundances of D and ${}^4\text{He}$ whose currently observed values are $(25.08 \pm 0.29) \times 10^{-6}$, and 0.245 ± 0.003 , respectively [10]. For example, if a BSM scenario produces additional neutrons, the ${}^7\text{Be}$ abundance can be reduced via ${}^7\text{Be}(n, p){}^7\text{Li}$, and the produced ${}^7\text{Li}$ gets subsequently destroyed by ${}^7\text{Li}(p, \alpha){}^4\text{He}$. As primordial ${}^7\text{Be}$ decays to ${}^7\text{Li}$ via the electron capture after recombination with the lifetime $\sim 5 \times 10^6$ sec, the current ${}^7\text{Li}$ (which is primordial ${}^7\text{Li} + {}^7\text{Be}$) can be reduced through this mechanism [35–44]. There are various ways to induce the excess neutrons: the direct decay of heavy particles, or indirectly through $p \rightarrow n$ conversion induced by injection of other particles such as mesons or neutrinos. However, this scenario inevitably increases the $p(n, \gamma)\text{D}$

* sganguly0205@ibs.re.kr

† thjung0720@gmail.com

‡ tspark@ibs.re.kr

§ csshin@cnu.ac.kr

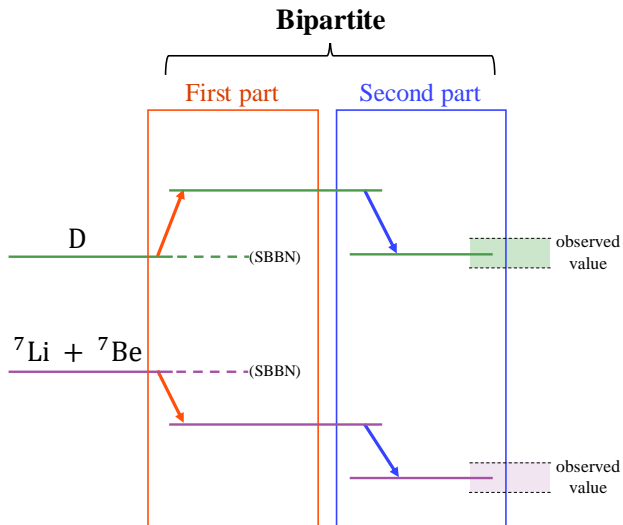


FIG. 1. Schematic picture of the bipartite solution.

rate due to the more neutrons, leading to an overproduction of D/H, and is thus ruled out after the precise measurement of D/H in [52–58]. Similarly, photon injection at a late time can lead to photo-dissociation of ${}^7\text{Be}$ and ${}^7\text{Li}$. However, the injected photons also destroy deuterium too much unless the energy of the injected photon lies in a narrow range between 1.59 MeV and 2.22 MeV (between D and ${}^7\text{Be}$ photo-dissociation thresholds) [48]. Thus, most of the parameter space in these simple solutions is already in severe tension with deuterium¹.

This apparent difficulty may stem from our tendency to favor simple or natural explanations, leading us to overlook possibilities that rely on accidental coincidences. In this work, we consider a solution composed of two distinct scenarios, which we call *bipartite solution* (see Fig. 1 for a schematic picture). The first part of our bipartite solution increases D and decreases ${}^7\text{Li} + {}^7\text{Be}$, while the second part decreases both D and ${}^7\text{Li} + {}^7\text{Be}$. Consequently, the effects on the D abundance from the two parts cancel each other, while ${}^7\text{Li} + {}^7\text{Be}$ can be reduced. As one can easily expect, this scenario requires tuning the abundances of two different particles so that the D abundance remains unchanged, and the goal of this paper is to quantify the degree of precision required for this balance. We do not include the theoretical uncertainty of D/H in our analysis, leading to a conservative estimation of the degree of tuning.

As a concrete example, we consider two late-time decaying particles: a majoron decaying into neutrinos, and an axion-like particle (ALP) decaying into photons. The majoron J couples with the standard model neutrinos

via $-\frac{g}{2}J\bar{\nu}_\alpha\gamma_5\nu_\alpha$ where $\alpha = e, \mu, \tau$, assuming the flavor universality as an approximation. The decay of J injects energetic neutrinos, and these neutrinos enhance the abundance of neutrons via $p \rightarrow n$ conversion. As discussed earlier, these excess neutrons can destroy ${}^7\text{Be}$, and explain the observed ${}^7\text{Li}$ abundance, but at the same time, D will be overproduced [44]. As the second decaying particle, an ALP ϕ couples with a pair of photons via $-\frac{g_{\alpha\gamma\gamma}}{4}\phi F^{\mu\nu}\tilde{F}_{\mu\nu}$. The photons produced from the ϕ decay destroy both D and ${}^7\text{Li} + {}^7\text{Be}$, bringing D back to the observed value while enhancing the depletion of the final ${}^7\text{Li}$ abundance.

In this work, we take the initial yields, $Y_J^{(0)}$ for J and $Y_\phi^{(0)}$ for ϕ , as free parameters, since they strongly depend on the reheating temperature and their UV completion. We also restrict the majoron mass $m_J \sim 100$ MeV for simplicity (neutrinos from a heavier majoron can produce muons, pions, etc.), and the ALP mass $m_\phi \sim 20$ MeV, which leads to the injected photon energy lying above the D threshold ~ 2 MeV but below the ${}^4\text{He}$ threshold ~ 20 MeV. If the photon energy were above the ${}^4\text{He}$ threshold, the photo-dissociation of ${}^4\text{He}$ leads to enhancing the D abundance, disabling the cancellation required for the observed D/H. In this case, our bipartite solution would not work.

For the majoron part to work properly, we need its lifetime τ_J to be around/after the deuterium bottleneck, $10 \text{ sec} \lesssim \tau_J \lesssim 10^4 \text{ sec}$ [44]. On the other hand, the lifetime of ϕ has to be greater than 10^5 sec to make injected photons efficiently destroy D and ${}^7\text{Li}$ before they get thermalized [60, 61]. Therefore, we have a hierarchy $\tau_J \ll \tau_\phi$, which indeed cleanly separates our analysis into two parts: (i) BBN evolution with J , and (ii) photo-dissociation driven by ϕ .

In part (i), we follow Ref. [44], ignoring the contribution from ϕ , which is a good approximation as long as ϕ 's initial abundance is sufficiently small (we check the consistency later on). This is reviewed in Sec. II A. We then take the boundary conditions obtained in part (i) and estimate the photo-dissociation processes in part (ii) mainly following Ref. [62], of which details are reviewed in Sec. II B. We combine these two parts and present our results in Sec. III, and conclude in Sec. IV.

II. EFFECTS OF PARTICLE INJECTION ON BBN

Decay products of a long-lived particle in BSM interact with light nuclei and also modify the background plasma evolution. This alters the prediction of SBBN, and the detailed effect depends on what particles are injected from the decay. Energetic neutrino injection alters the neutron-proton freeze-out process, or directly interacts with nuclei depending on the lifetime of the BSM particle [42–44, 63–66]. If the decay products are e^\pm or γ , energetic photons at around or after 10^5 sec can photo-

¹ Including the theoretical uncertainty of D/H, which is roughly 5% [59], can, in principle, mitigate the difficulty, but does not rescue these solutions.

dissociate D, ${}^4\text{He}$, and ${}^3\text{He}$ [60–62, 67–76]. As discussed in Refs. [35–37, 41, 73, 77–97], hadronic injections can significantly modify the predictions of SBBN. For the purpose of our study, we only discuss two specific scenarios: i) neutrino injection from majoron decay, and ii) photon injection from the ALP decay.

Modified evolution of a nucleus $A = p, n, \text{D}, \dots$ can be obtained by solving

$$\frac{dX_A}{dt} = \Gamma_A^{\text{SBBN}} - \sum_{B \neq A} \left[\delta\Gamma_{A \rightarrow B} X_A - \delta\Gamma_{B \rightarrow A} X_B \right], \quad (1)$$

where $X_A = n_A/n_b$ is the ratio of A number density n_A and the total baryon number density n_b , and Γ_A^{SBBN} denotes the production rate of A in SBBN, which is a function of the abundances of other species.

The second term on the right-hand side (RHS) of Eq. (1) corresponds to the BSM effects. For $\delta\Gamma_{A \rightarrow B}$ and $\delta\Gamma_{B \rightarrow A}$, it is crucial to obtain non-thermal distributions of injected neutrinos ν_{nt} or photons γ_{nt} , which we denote $f_{\nu_{\text{nt}}}$ and $f_{\gamma_{\text{nt}}}$, respectively, as well as modified background plasma properties such as background neutrino temperature. In the following subsections, we describe the derivation of these functions and examine their impact on the background plasma evolution.

A. Part I: early-time neutrino injection

The decay of majoron produces energetic neutrinos with initial energy $m_J/2$. The neutrino momentum distribution function $f_{\nu_{\text{nt},\alpha}}$ for a flavor $\alpha = e, \mu, \tau$ can be obtained by solving the Boltzmann equation

$$\frac{\partial f_{\nu_{\text{nt},\alpha}}}{\partial t} - Hp \frac{\partial f_{\nu_{\text{nt},\alpha}}}{\partial p} = \frac{2\pi^2 n_J}{3E^2 \tau_J} \delta\left(E - \frac{m_J}{2}\right) - \mathcal{C}_{\nu_{\text{nt},\alpha}}, \quad (2)$$

where H is the Hubble expansion rate and $p \equiv |\vec{p}|$ and E are the magnitude of the three-momentum and energy of $\nu_{\text{nt},\alpha}$, respectively. The first term on the RHS corresponds to the source term of $\nu_{\text{nt},\alpha}$ from the majoron decay, with its number density denoted by n_J . For simplicity, we approximate $n_J(T) = Y_J^{(0)} s(T) \exp(-t/\tau_J)$ where $s(T)$ is the entropy density of the background plasma.

The last term of Eq. (2) generates the reduction of the number of $f_{\nu_{\text{nt},\alpha}}$ due to its scattering with the background electrons and neutrinos, ignoring their asymmetry and the contribution from the baryons. The explicit form of $\mathcal{C}_{\nu_{\text{nt},\alpha} a \rightarrow bc}$ is written as

$$\mathcal{C}_{\nu_{\text{nt},\alpha}} = \sum_{a,b,c} \frac{S f_{\nu_{\text{nt},\alpha}}}{2E} \int d\Pi_a d\Pi_b d\Pi_c |\mathcal{M}_{\nu_{\text{nt},\alpha} a \rightarrow bc}|^2 f_a (2\pi)^4 \delta^4(P + P_a - P_b - P_c). \quad (3)$$

Here a, b , and c denote the background particles e^+, e^-, ν or $\bar{\nu}$ with their four momenta P_a, P_b , and P_c . $\mathcal{M}_{\nu_{\text{nt},\alpha} a \rightarrow bc}$

is matrix amplitude of the process $\nu_{\text{nt},\alpha} a \rightarrow bc$ and S is its symmetry factor. $d\Pi_i = d^3\vec{p}_i / (2\pi)^3 2E_i$ is the Lorentz-invariant phase space measure and f_a is the momentum distribution of the initial state particle a . The explicit form of the matrix amplitude for different processes can be found in Appendix A of Ref. [44].

In Eq. (2), we dropped positive scattering terms that come from the elastic scattering processes as an approximation. This is equivalent to assuming that a non-thermal neutrino gets thermalized by a single scattering, which leads to an underestimated number of $\nu_{\text{nt},\alpha}$ in the intermediate energy range. However, for $\nu_{\text{nt},\alpha}$ to efficiently produce neutrons, which are the key ingredient to reduce ${}^7\text{Li} + {}^7\text{Be}$, we need the collision terms to be small enough, leading us to $\tau_J \gtrsim 10$ sec. Thus, the positive scattering terms are also suppressed in this range, and thus neglecting them is a good approximation.

$f_{\nu_{\text{nt},\alpha}}$ modifies the BBN evolution via $\delta\Gamma_{A \rightarrow B}$ in Eq. (1) with

$$\delta\Gamma_{A \rightarrow B} = \frac{1}{2\pi^2} \int dE_{\nu_{\text{nt}}} E_{\nu_{\text{nt}}}^2 f_{\nu_{\text{nt}}}(\sigma v)_{\nu_{\text{nt}} A \rightarrow B} + \Delta\Gamma_{A \rightarrow B}^{(\text{weak})}, \quad (4)$$

where $\sigma_{\nu_{\text{nt}} A \rightarrow B}$ is the scattering cross section of ν_{nt} and A which produces B . The last term $\Gamma_{A \rightarrow B}^{(\text{weak})}$ accounts for the effect coming from the modified temperature of the background neutrinos, which can affect $n \leftrightarrow p$ conversion processes. We include this effect although it is negligible for $\tau_J \gtrsim 10$ sec [44].

In addition, non-thermal neutrinos transfer part of their energy to the $e\gamma B$ sector through scatterings with the background plasma, and this effect is taken into account in the evolution of $\rho_{e\gamma B}$ through the modified Boltzmann equation

$$\dot{\rho}_{e\gamma B} + 3H(\rho_{e\gamma B} + P_{e\gamma B}) = -T^4 H(T) (\mathcal{N}(T) + \Delta\mathcal{N}(T)), \quad (5)$$

where $P_{e\gamma B}$ is the pressure of the $e\gamma B$ sector. The effect of the non-instantaneous neutrino decoupling in SBBN is encoded in $\mathcal{N}(T)$ term [98–100] on the RHS and $\Delta\mathcal{N}(T)$ is its correction in the presence of ν_{nt} , which is given by

$$\Delta\mathcal{N}(T) = \sum_{\alpha} \frac{\Gamma(\nu_{\text{nt},\alpha} \rightarrow e) \rho_{\nu_{\text{nt},\alpha}}(T)}{H(T) T^4}. \quad (6)$$

Here $\rho_{\nu_{\text{nt},\alpha}}(T)$ is the energy density of non-thermal neutrinos, and $\Gamma(\nu_{\text{nt},\alpha} \rightarrow e)$ is the effective rate for energy transfer from $\nu_{\text{nt},\alpha}$ to the electromagnetic plasma, whose explicit form is given in Appendix A of Ref. [44].

Energy transfer from ν_{nt} to $e\gamma B$ sector also dilutes the baryon-to-photon ratio η_B . To fix its final value after the BBN epoch as $\eta_{B,\text{fin}} = 6.1 \times 10^{-10}$ to agree with CMB fitting [5], we modify the initial baryon asymmetry as

$$\frac{\eta_{B,\text{ini}}}{\eta_{B,\text{fin}}} = \left[2.73 - \frac{45}{2\pi^2 g_* s(T_f)} \int_{T_{\nu d}}^{T_f} \sum_{\alpha} \frac{\Gamma(\nu_{\text{nt},\alpha} \rightarrow e) \rho_{\nu_{\text{nt},\alpha}}(T)}{H(T) T^2 T_{\nu_{\text{bg}}}^3} dT \right], \quad (7)$$

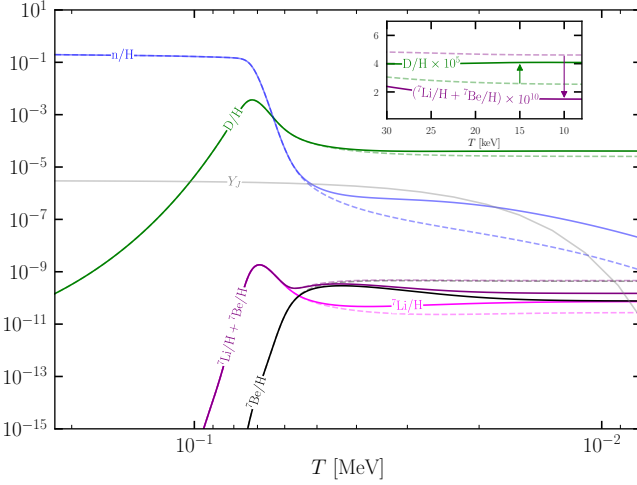


FIG. 2. Evolution of n/H (blue), D/H (green), ${}^7\text{Li}/H$ (magenta), ${}^7\text{Be}/H$ (black), $({}^7\text{Li}/H + {}^7\text{Be}/H) \times 10^{10}$ (purple), and Y_J (gray) as a function of T for $m_J = 100$ MeV, $\tau_J = 10^3$ sec, and $Y_J^{(0)} = 3 \times 10^{-6}$. The dashed lines depict their evolution in SBBN.

where $T_{\nu_{\text{bg}}}$ is the background neutrino temperature and we take $T_{\nu_{\text{d}}} = 2.3$ MeV and $T_f = 5$ keV.

In Fig. 2, we show the evolution of light element abundances in T for $m_J = 100$ MeV, $Y_J^{(0)} = 3 \times 10^{-6}$, and $\tau_J = 10^3$ sec. Different colored lines correspond to different elements, as indicated by labels in each line, and the dashed lines represent the evolution in SBBN. As discussed earlier, the $p \rightarrow n$ conversion rate is enhanced due to the injection of energetic neutrinos from majoron decay, leading to an enhanced neutron density (see the blue lines). These additional neutrons subsequently make the deuterium production more efficient through the $p(n, \gamma)D$ reaction, resulting in a larger D/H in comparison to its SBBN value (see the green lines). On the other hand, the effect of these additional neutrons on ${}^7\text{Li} + {}^7\text{Be}$ abundance is opposite. The excess neutrons dissociate ${}^7\text{Be}$ through ${}^7\text{Be}(n, p){}^7\text{Li}$, and the produced ${}^7\text{Li}$ is subsequently converted into ${}^4\text{He}$ via ${}^7\text{Li}(p, {}^4\text{He}){}^4\text{He}$. As a result of the ${}^7\text{Be}$ dissociation, the final ${}^7\text{Li} + {}^7\text{Be}$ abundance (solid purple line) is smaller than its SBBN value (dashed purple line).

We depict in Fig. 3 (taken from [44]) the constraints in $\tau_J - Y_J^{(0)}$ plane for $m_J = 100$ MeV, assuming that there is no second part. The constraints from the overabundance of D , ${}^4\text{He}$, and ${}^3\text{He}$ correspond to the green, blue, and magenta regions, respectively, and a rough estimation of ΔN_{eff} constraint is shown by the gray shaded region. The supernova 1987A constraint from [101] is also depicted by the light blue shaded region, where we use the relation $\tau_J \simeq 16\pi/3g^2 m_J$ with an approximation of flavor universal decay.

Importantly, the region surrounded by the purple dotted curves in Fig. 3 corresponds to the parameter space where the observed ${}^7\text{Li}$ can be explained. However, as we pointed out in the introduction, this region is already ex-

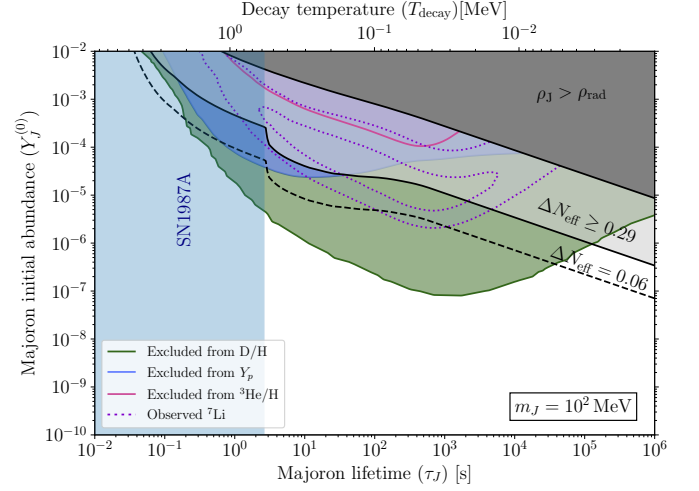


FIG. 3. BBN constraint on $\tau_J - Y_J^{(0)}$ plane for $m_J = 100$ MeV, taken from [44]. Exclusion limit at 95% confidence level (C.L.) from D , ${}^4\text{He}$, and ${}^3\text{He}$ are depicted by green, blue, and magenta colored regions, respectively. The dark gray region is excluded from the majoron domination during/after BBN. The observed value of lithium abundance can be explained in the parameter region outlined by purple dotted lines. ΔN_{eff} constraint from Planck 2018 and future experiment CMB-S4 [102] is depicted by black solid and dashed lines, respectively. The light blue region is excluded from SN 1987A constraint.

cluded by the overproduction of D . This will be resolved by combining with the second part, where injected photons reduce both D and ${}^7\text{Li} + {}^7\text{Be}$ abundances.

B. Part II: late-time photon injection

In the second part, photons injected from the decay of ALP, each with initial energy $E_0 = m_\phi/2$, scatter off the background photons and charged particles. These interactions initiate electromagnetic (EM) cascades, leading to the production of secondary photons and electrons/positrons with lower energies.

Following Ref. [61], the momentum distributions of γ_{nt} , e_{nt}^- , and e_{nt}^+ can be obtained by solving the Boltzmann equations,

$$\begin{aligned}
 \frac{\partial \hat{f}_{\gamma_{\text{nt}}}}{\partial t} - H p \frac{\partial \hat{f}_{\gamma_{\text{nt}}}}{\partial p} &= \xi_\gamma \delta(E - E_0) - \Gamma_\gamma \hat{f}_{\gamma_{\text{nt}}} \\
 &+ \int_E^{E_0} dE'_\gamma \hat{f}_{\gamma_{\text{nt}}}(E'_\gamma) K_{\gamma \rightarrow \gamma}(E'_\gamma, E) \\
 &+ \int_E^{E_0} dE'_{e^-} \hat{f}_{e_{\text{nt}}^-}(E'_{e^-}) K_{e^- \rightarrow \gamma}(E'_{e^-}, E) \\
 &+ \int_E^{E_0} dE'_{e^+} \hat{f}_{e_{\text{nt}}^+}(E'_{e^+}) K_{e^+ \rightarrow \gamma}(E'_{e^+}, E),
 \end{aligned} \tag{8}$$

$$\begin{aligned}
\frac{\partial \hat{f}_{e_{\text{nt}}^-}}{\partial t} - Hp \frac{\partial \hat{f}_{e_{\text{nt}}^-}}{\partial p} &= -\Gamma_{e^-} \hat{f}_{e_{\text{nt}}^-} \\
&+ \int_E^{E_0} dE'_\gamma \hat{f}_{\gamma_{\text{nt}}}(E'_\gamma) K_{\gamma \rightarrow e^-}(E'_\gamma, E) \\
&+ \int_E^{E_0} dE'_{e^-} \hat{f}_{e_{\text{nt}}^-}(E'_{e^-}) K_{e^- \rightarrow e^-}(E'_{e^-}, E), \\
\end{aligned} \tag{9}$$

$$\begin{aligned}
\frac{\partial \hat{f}_{e_{\text{nt}}^+}}{\partial t} - Hp \frac{\partial \hat{f}_{e_{\text{nt}}^+}}{\partial p} &= -\Gamma_{e^+} \hat{f}_{e_{\text{nt}}^+} \\
&+ \int_E^{E_0} dE'_\gamma \hat{f}_{\gamma_{\text{nt}}}(E'_\gamma) K_{\gamma \rightarrow e^+}(E'_\gamma, E) \\
&+ \int_E^{E_0} dE'_{e^+} \hat{f}_{e_{\text{nt}}^+}(E'_{e^+}) K_{e^+ \rightarrow e^+}(E'_{e^+}, E), \\
\end{aligned} \tag{10}$$

where we denote $\hat{f}_a \equiv \frac{dn_a}{dE} = g_a \frac{p^2}{2\pi^2} \frac{dp}{dE} f_a$ as energy distribution of species $a = \gamma_{\text{nt}}, e_{\text{nt}}^-$ and e_{nt}^+ with its number of degrees of freedom g_a . $K_{a \rightarrow b}(E', E)$ corresponds to differential scattering rate of initial state a with energy E' becoming b with energy E , while Γ_a is the total reaction rate of a . We take $K_{a \rightarrow b}$ and Γ_a from Appendix B of Ref. [61], where injected photon energy is assumed to be much greater than the background photon energy. The first term on the RHS of Eq. (8) is the source term with $\xi_\gamma = 2n_\phi(t)/\tau_\phi$. We approximate the ϕ number density $n_\phi(t) = Y_\phi^{(0)} s(T) \exp(-t/\tau_\phi)$, taking its initial yield $Y_\phi^{(0)}$ and lifetime τ_ϕ free parameters.

Since the time scale of the scattering processes is much shorter than the Hubble time scale [60], we can take stationary solutions which can be obtained by taking $\partial f_a / \partial t = 0$ in Eq. (8)–(10);

$$\begin{aligned}
\Gamma_{\gamma_{\text{nt}}}(E) F_{\gamma_{\text{nt}}}(E) &= \frac{\xi_\gamma K_{\gamma \rightarrow \gamma}(E^0, E)}{\Gamma_\gamma(E_0)} \\
&+ \int_E^{E_0} dE'_\gamma K_{\gamma \rightarrow \gamma}(E'_\gamma, E) F_{\gamma_{\text{nt}}}(E'_\gamma) \\
&+ \int_E^{E_0} dE'_{e^-} K_{e^- \rightarrow \gamma}(E'_{e^-}, E) F_{e_{\text{nt}}^-}(E'_{e^-}) \\
&+ \int_E^{E_0} dE'_{e^+} K_{e^+ \rightarrow \gamma}(E'_{e^+}, E) F_{e_{\text{nt}}^+}(E'_{e^+}), \\
\end{aligned} \tag{11}$$

$$\begin{aligned}
\Gamma_{e^-}(E) F_{e_{\text{nt}}^-}(E) &= \frac{\xi_\gamma K_{\gamma \rightarrow e^-}(E_0, E)}{\Gamma_\gamma(E_0)} \\
&+ \int_E^{E_0} dE'_\gamma K_{\gamma \rightarrow e^-}(E'_\gamma, E) F_{\gamma_{\text{nt}}}(E'_\gamma) \\
&+ \int_E^{E_0} dE'_{e^-} K_{e^- \rightarrow e^-}(E'_{e^-}, E) F_{e_{\text{nt}}^-}(E'_{e^-}), \\
\end{aligned} \tag{12}$$

$$\Gamma_{e^+}(E) F_{e_{\text{nt}}^+}(E) = \frac{\xi_\gamma K_{\gamma \rightarrow e^+}(E_0, E)}{\Gamma_\gamma(E_0)}$$

where we define

$$\begin{aligned}
F_{\gamma_{\text{nt}}}(E) &= \hat{f}_{\gamma_{\text{nt}}} - \frac{\xi_\gamma \delta(E - E_0)}{\Gamma_{\gamma_{\text{nt}}}(E)}, \\
F_{e_{\text{nt}}^-}(E) &= \hat{f}_{e_{\text{nt}}^-}, \\
F_{e_{\text{nt}}^+}(E) &= \hat{f}_{e_{\text{nt}}^+}. \\
\end{aligned} \tag{14}$$

To obtain F_a numerically, we discretize the energy interval $E_{\text{min}} \leq E_\gamma, E_{e^-}$, and $E_{e^+} \leq E_0$ into N bins, and write the $F_{\gamma_{\text{nt}}}(E_i)$, $F_{e_{\text{nt}}^-}(E_i)$, and $F_{e_{\text{nt}}^+}(E_i)$ for $0 \leq i \leq N$ as

$$\begin{aligned}
F_{\gamma_{\text{nt}}}(E_i) &= \frac{1}{\Gamma_{\gamma_{\text{nt}}}(E_i)} \left[\frac{\xi_\gamma K_{\gamma \rightarrow \gamma}(E_0, E_i)}{\Gamma_{\gamma_{\text{nt}}}(E^0)} \right. \\
&+ \sum_{\substack{E_N=E_0 \\ E_j > E_i}} \Delta E_j K_{\gamma \rightarrow \gamma}(E_j, E_i) F_{\gamma_{\text{nt}}}(E_j) \\
&+ \sum_{\substack{E_N=E_0 \\ E_j > E_i}} \Delta E_j K_{e^- \rightarrow \gamma}(E_j, E_i) F_{e_{\text{nt}}^-}(E_j) \\
&+ \left. \sum_{\substack{E_N=E_0 \\ E_j > E_i}} \Delta E_j K_{e^+ \rightarrow \gamma}(E_j, E_i) F_{e_{\text{nt}}^+}(E_j) \right], \\
\end{aligned} \tag{15}$$

$$\begin{aligned}
F_{e_{\text{nt}}^-}(E_i) &= \frac{1}{\Gamma_{e_{\text{nt}}^-}(E_i)} \left[\frac{\xi_\gamma K_{\gamma \rightarrow e^-}(E_0, E_i)}{\Gamma_{\gamma_{\text{nt}}}(E^0)} \right. \\
&+ \sum_{\substack{E_N=E_0 \\ E_j > E_i}} \Delta E_j K_{\gamma \rightarrow e^-}(E_j, E_i) F_{\gamma_{\text{nt}}}(E_j) \\
&+ \left. \sum_{\substack{E_N=E_0 \\ E_j > E_i}} \Delta E_j K_{e^- \rightarrow e^-}(E_j, E_i) F_{e_{\text{nt}}^-}(E_j) \right], \\
\end{aligned}$$

$$\begin{aligned}
F_{e_{\text{nt}}^+}(E_i) &= \frac{1}{\Gamma_{e_{\text{nt}}^+}(E_i)} \left[\frac{\xi_\gamma K_{\gamma \rightarrow e^+}(E_0, E_i)}{\Gamma_{\gamma_{\text{nt}}}(E^0)} \right. \\
&+ \sum_{\substack{E_N=E_0 \\ E_j > E_i}} \Delta E_j K_{\gamma \rightarrow e^+}(E_j, E_i) F_{\gamma_{\text{nt}}}(E_j) \\
&+ \left. \sum_{\substack{E_N=E_0 \\ E_j > E_i}} \Delta E_j K_{e^+ \rightarrow e^+}(E_j, E_i) F_{e_{\text{nt}}^+}(E_j) \right], \\
\end{aligned} \tag{16}$$

where $\Delta E_j = (E_{j+1} - E_{j-1})/2$.

Photons that maintain energy higher than nuclei's photo-dissociation thresholds can dissociate light elements such as D, ${}^7\text{Be}$, etc., which is required for the second part of our bipartite solution (recall Fig. 1). However, they lose their energy via $\gamma_{\text{nt}} + \gamma \rightarrow e^+ + e^-$ rapidly

if the energy is higher than $m_e^2/20T$. Thus, we only consider the injection time $\gtrsim 10^5$ sec (at temperature $\lesssim 10$ keV), where the nuclear reaction chain has already been turned off, $\Gamma_A^{\text{SBBN}} \simeq 0$ in Eq. (1). When the injection time is earlier, $f_{\gamma_{\text{nt}}}$ is extremely suppressed due to rapid thermalization, and thus it has no impact other than the entropy injection to the photon sector.

The Boltzmann equations for the evolution of D, ${}^7\text{Li}$, and ${}^7\text{Be}$ in the presence of ALP are given by

$$\begin{aligned} \frac{dX_{\text{D}}}{dt} &= -X_{\text{D}}\Gamma_{\text{D}\gamma\rightarrow p\text{n}}, \\ \frac{dX_{{}^7\text{Li}}}{dt} &= -X_{{}^7\text{Li}}(\Gamma_{{}^7\text{Li}\gamma\rightarrow {}^3\text{He}^4\text{He} + \Gamma_{{}^7\text{Li}\gamma\rightarrow n^6\text{Li}} + \Gamma_{{}^7\text{Li}\gamma\rightarrow np^4\text{He}}), \\ \frac{dX_{{}^7\text{Be}}}{dt} &= -X_{{}^7\text{Be}}\Gamma_{{}^7\text{Be}\gamma\rightarrow {}^3\text{He}^4\text{He}}. \end{aligned} \quad (17)$$

Restricting m_ϕ to be smaller than twice of ${}^4\text{He}$ photo-dissociation threshold ($= 19.81$ MeV for the ${}^4\text{He} + \gamma \rightarrow p + \text{T}$ channel), we ignore dissociation of ${}^4\text{He}$, and abundances of outgoing particles after ${}^7\text{Li}$ and ${}^7\text{Be}$ dissociation are negligible. We do not take into account T and ${}^3\text{He}$ since measurements of primordial ${}^3\text{He}$ abundance have a large uncertainty (see, e.g., [103, 104]) and only an upper bound is meaningful. Note, however, that if the photon energy were greater than the ${}^4\text{He}$ photo-dissociation threshold, T and ${}^3\text{He}$ could be overproduced as remnants of ${}^4\text{He}$ photo-dissociation leading to another strong bound. We do not consider that case as we take $m_\phi \lesssim 40$ MeV. The reaction rate $\Gamma_{\gamma_{\text{nt}j}\rightarrow kl}$ for a process $\gamma_{\text{nt}j} \rightarrow kl$ can be written as

$$\begin{aligned} \Gamma_{\gamma_{\text{nt}j}\rightarrow kl} &= \frac{\xi_\gamma \sigma_{\gamma_{\text{nt}j}\rightarrow kl}(E_0)}{\Gamma_{\text{nt}}(E_0)} \\ &+ \int_{E_{\text{min}}}^{E_0} dE_{\gamma_{\text{nt}}} F_{\gamma_{\text{nt}}}(E_{\gamma_{\text{nt}}}) \sigma_{\gamma_{\text{nt}j}\rightarrow kl}(E_{\gamma_{\text{nt}}}), \end{aligned} \quad (18)$$

where $\sigma_{\gamma_{\text{nt}j}\rightarrow kl}(E_{\gamma_{\text{nt}}})$ is the scattering cross section of $\gamma_{\text{nt}j} \rightarrow kl$. In our analysis, we take cross sections from the JENDL library data for the photo dissociation of D [105] and re-derived the fitting formulae for ${}^7\text{Li}$ and ${}^7\text{Be}$ cross sections, as summarized in Appendix A.

The decay of ϕ injects entropy into the photon bath and thus modifies the evolution of the background photon temperature. The evolution equation is given by

$$\frac{\dot{T}}{T} = \frac{\Gamma_\phi \rho_\phi}{4\rho_\gamma} - H, \quad (19)$$

where $\rho_\gamma = 2\frac{\pi^2}{30}T^4$ and $\rho_\phi \simeq m_\phi n_\phi$ are energy densities of the background photon and ϕ .

In Fig. 4, we show the evolution of D/H (green), ${}^7\text{Li}/\text{H}$ (magenta), ${}^7\text{Be}/\text{H}$ (black), $({}^7\text{Li} + {}^7\text{Be})/\text{H}$ (purple), and Y_ϕ (gray) for the SBBN case (dashed) and the ALP case (solid) with $m_\phi = 20$ MeV, $Y_\phi^{(0)} = 10^{-9}$, and $\tau_\phi = 10^6$ sec. Since the injected energy is larger than the photo-dissociation threshold of D, ${}^7\text{Li}$, and ${}^7\text{Be}$, non-thermal photons can destroy D, ${}^7\text{Li}$, and ${}^7\text{Be}$.

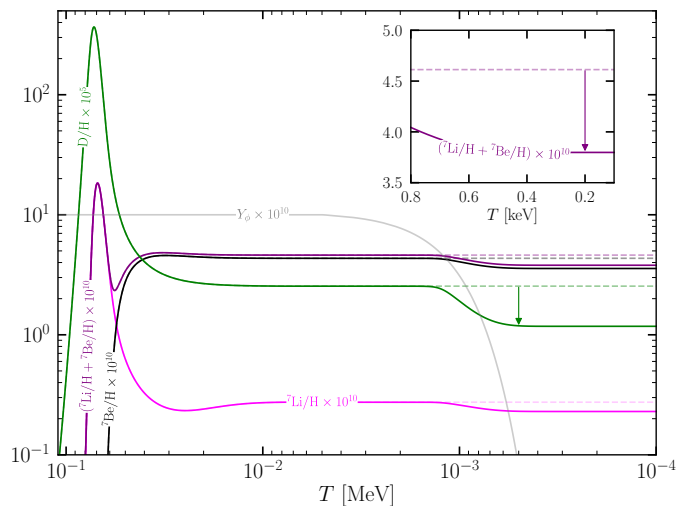


FIG. 4. Evolution of D/H (green), ${}^7\text{Li}/\text{H}$ (magenta), ${}^7\text{Be}/\text{H}$ (black), $({}^7\text{Li} + {}^7\text{Be})/\text{H}$ (purple), and Y_ϕ (gray) are shown as a function of T for $m_\phi = 20$ MeV, $\tau_\phi = 10^6$ sec, and $Y_\phi^{(0)} = 10^{-9}$. The dashed lines depict their evolution in SBBN.

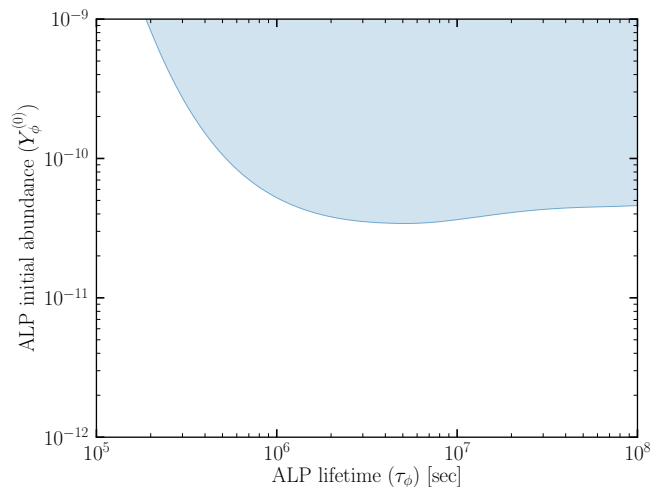


FIG. 5. BBN constraint on $\tau_\phi - Y_\phi^{(0)}$ plane for $m_\phi = 20$ MeV. The light blue region is excluded from the deuterium abundance at 95% C.L.

If the first part of our scenario is absent, the deuterium photo-dissociation provides a strong constraint. In Fig. 5, we depict our numerical estimation of the constraint (shaded blue region) for $m_\phi = 20$ MeV in $\tau_\phi - Y_\phi^{(0)}$ plane. As one can see, the constraint becomes significantly weaker when $\tau_\phi < 10^6$ sec due to the rapid thermalization of injected photons. For $\tau_\phi \gtrsim 10^6$, photons are essentially collision-free, and most of the emitted photons can efficiently induce photodissociation. Consequently, the bound on the initial abundance shows only a weak dependence on τ_ϕ , becoming nearly flat in this regime.

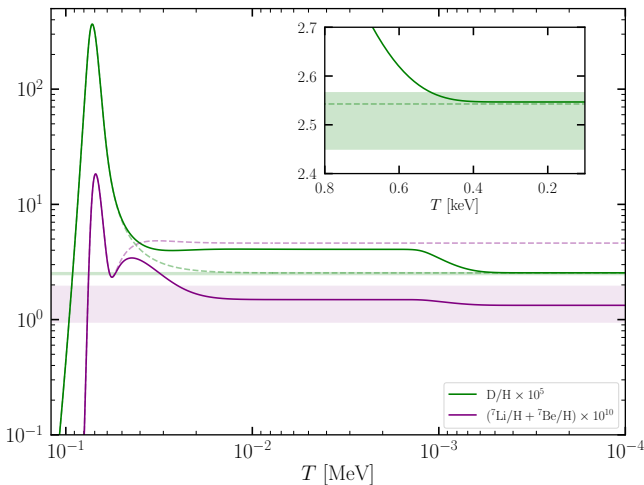


FIG. 6. Evolution of D/H (green) and ${}^7\text{Li}/\text{H} + {}^7\text{Be}/\text{H}$ (purple) as a function of T . The dashed lines depict their evolution for the SBBN scenario. The observational limits of D/H and $({}^7\text{Li}/\text{H} + {}^7\text{Be}/\text{H})$ at 95% C.L. are shown by green and purple bands, respectively. Here, we choose $(m_J, \tau_J, Y_J^{(0)}) = (100 \text{ MeV}, 10^3 \text{ sec}, 3 \times 10^{-6})$, and $(m_\phi, \tau_\phi, Y_\phi^{(0)}) = (20 \text{ MeV}, 10^6 \text{ sec}, 6.1 \times 10^{-10})$ to solve the lithium problem while satisfying the constraint on D/H abundance.

III. SOLUTION TO THE LITHIUM PROBLEM

Let us now combine the majoron part and the ALP part together, and show how our bipartite solution works. We first obtain the light nuclei abundances in the majoron part, and they are taken as a boundary condition for the ALP part to obtain their final abundances.

In Fig. 6, we show the evolution of D/H, and $({}^7\text{Li} + {}^7\text{Be})/\text{H}$ in temperature T , taking benchmark parameters $(m_J, \tau_J, Y_J^{(0)}) = (100 \text{ MeV}, 10^3 \text{ sec}, 3 \times 10^{-6})$, and $(m_\phi, \tau_\phi, Y_\phi^{(0)}) = (20 \text{ MeV}, 10^6 \text{ sec}, 6.1 \times 10^{-10})$. These parameters are selected to solve the cosmological lithium problem, while satisfying the constraint on D/H. As one can see from the figure, $({}^7\text{Li} + {}^7\text{Be})/\text{H}$ is reduced and D/H is enhanced by the decay of majoron at temperature around 100 – 10 keV. Then, later-time decay of ALP counterbalances the excess D from the majoron decay, and D/H gets back to the 2σ band of D/H. $({}^7\text{Li} + {}^7\text{Be})/\text{H}$ is also further reduced by the ALP, but remains within the 2σ band.

Scanning the whole parameter space is technically challenging because we have in total six free parameters: $m_J, \tau_J, Y_J^{(0)}, m_\phi, \tau_\phi$, and $Y_\phi^{(0)}$. Thus, we coarsely scan the parameter space and fit the numerical result with analytic formulae of D/H and ${}^7\text{Li}/\text{H}$. The effect from the majoron decay on D and ${}^7\text{Li}$ can be approximated linearly in $Y_J^{(0)}$ since their overproduction is additive. We numerically checked that including a quadratic order does not improve the goodness of fitting a lot. On the other hand, majoron’s effect on ${}^7\text{Be}$ should be treated as

an exponential suppression because destruction always requires itself. Similarly, the photo-dissociation effects from $Y_\phi^{(0)}$ in both D and ${}^7\text{Li}$ abundances can be treated as an exponential suppression form in Y_ϕ . This physical picture motivates the following fitting ansatz for a given τ_J and τ_ϕ :

$$(\text{D}/\text{H})_{\text{fin.}} = (a_1 + b_1 Y_J^{(0)}) \exp(-c_1 Y_\phi^{(0)}), \quad (20)$$

$$({}^7\text{Li}/\text{H})_{\text{fin.}} = a_2 \left(\exp(-b_2 Y_J^{(0)}) + c_2 Y_J^{(0)} \right) \exp(-d_2 Y_\phi^{(0)}). \quad (21)$$

Here, the subscript “fin” stands for the value estimated at the current Universe and fitting parameters a_i, b_i, c_i , and d_i depend on both mass (m_J, m_ϕ) and lifetime (τ_J, τ_ϕ) in general. Choosing $m_J = 100 \text{ MeV}$ and $m_\phi = 20 \text{ MeV}$ (which are taken as a benchmark hereafter since dependence on masses is mild) and taking numerical results in $10^{-7} \leq Y_J^{(0)} \leq 10^{-5}$, $10^{-10} \leq Y_\phi^{(0)} \leq 10^{-7}$, $10 \text{ sec} \leq \tau_J \leq 10^5 \text{ sec}$, $10^5 \text{ sec} \leq \tau_\phi \leq 10^8 \text{ sec}$, we obtain fitting parameters summarized in Table I in Appendix B. We find that b_1, b_2 , and c_2 strongly depend on τ_J , but are not sensitive to τ_ϕ . Similarly, c_1 and d_2 are sensitive to τ_ϕ , but remain insensitive to τ_J . When $\tau_\phi \gtrsim 10^6 \text{ sec}$, c_1 and d_2 become almost independent of τ_ϕ .

In Fig. 7 we fix τ_J and τ_ϕ , and find parameter region in $Y_J^{(0)} - Y_\phi^{(0)}$ plane where ${}^7\text{Li}$ (purple) and D (green) abundances can fit within 2σ range. Thus, the overlapped region is where the lithium problem is solved. We take $\tau_J = 10^2 \text{ sec}$, $\tau_\phi = 10^7 \text{ sec}$ in the left panel and $\tau_J = 10^3 \text{ sec}$, $\tau_\phi = 10^7 \text{ sec}$ in the right panel. In both panels, the contours derived from the numerical data are shown by the solid lines, whereas those derived from our fitting formulae, given in Eq. (20) and (21) are shown by the dashed lines. As illustrated in the figure, the parameter space derived from the fitting formulae shows good agreement with that obtained from the numerical data. As indicated by the narrowness of the overlapped region, we need $\sim 10\%$ tuning of $Y_\phi^{(0)}$ for an $O(1)$ range of $Y_J^{(0)}$.

To see the τ_J dependence of our working parameter space, in Fig. 8, we fix $\tau_\phi = 10^6 \text{ sec}$, tune $Y_\phi^{(0)}$ to give the observed central value of D/H, and depict ${}^7\text{Li}/\text{H}$ by gray contours. The shaded region is where the lithium problem is solved up to 2σ . As expected in the Sec. II A, a wide range of τ_J is allowed; $10 \text{ sec} \lesssim \tau_J \lesssim 10^4 \text{ sec}$.

Similarly, in Fig. 9, we take $Y_J^{(0)}$ tuned for D/H with $\tau_J = 10^3 \text{ sec}$, and show ${}^7\text{Li}/\text{H}$ by gray contours with shaded region representing the solution to the lithium problem up to 2σ . For $\tau_\phi \lesssim 10^6 \text{ sec}$, the required value of $Y_\phi^{(0)}$ to solve the lithium problem is significantly large due to the rapid thermalization of injected photons. It becomes insensitive to τ_ϕ if $\tau_\phi \gtrsim 10^6 \text{ sec}$.

As a final result, for each τ_J and τ_ϕ , we find best fit values of $Y_J^{(0)}$ and $Y_\phi^{(0)}$ for D/H and ${}^7\text{Li}/\text{H}$, which are depicted by brown and blue contours in Fig. 10. For $\tau_J \gtrsim 4 \times 10^3 \text{ sec}$, the parameter space that could potentially solve the lithium problem is excluded by the

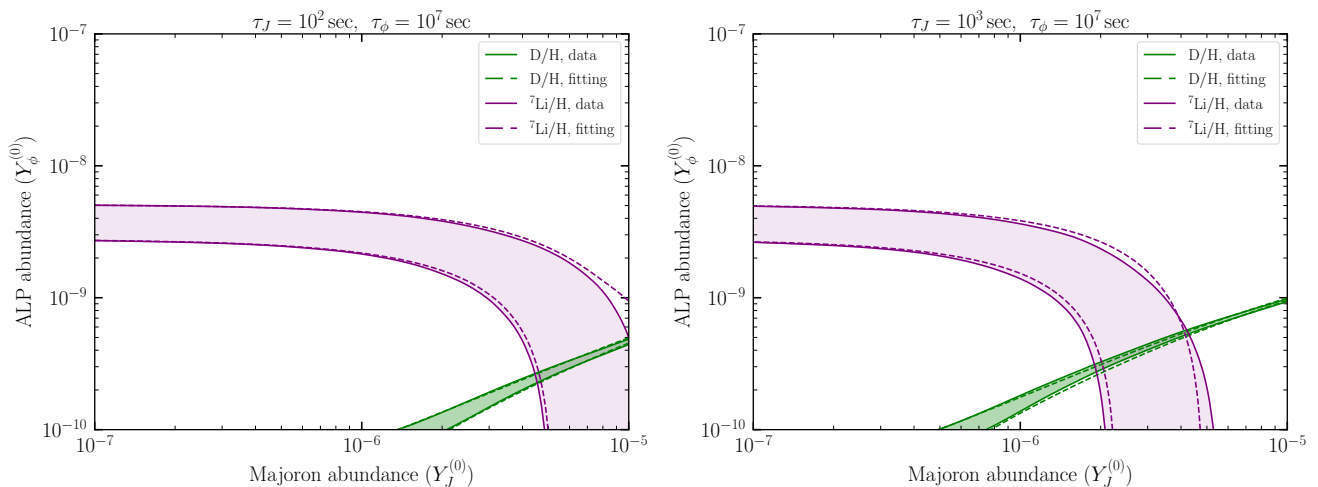


FIG. 7. Parameter space in $Y_J^{(0)} - Y_\phi^{(0)}$ plane to explain the observed ${}^7\text{Li}$ (purple) and D (green) within 95% C.L. for $(\tau_J, \tau_\phi) = (10^2 \text{ sec}, 10^7 \text{ sec})$ (left panel) and $(10^3 \text{ sec}, 10^7 \text{ sec})$ (right panel). In both panels, we consider $m_J = 100 \text{ MeV}$ and $m_\phi = 20 \text{ MeV}$. Solid contours represent our numerical data, whereas dashed contours correspond to fitting formulae (20) and (21) using the parameters in Table I.

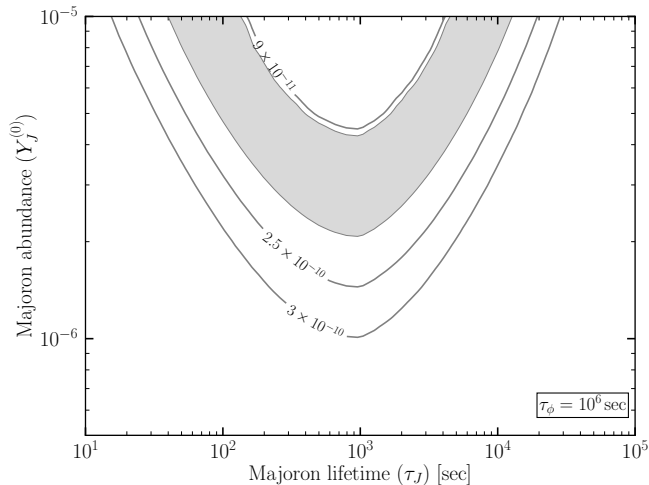


FIG. 8. Working parameter space in $\tau_J - Y_J^{(0)}$ plane for $\tau_\phi = 10^6 \text{ sec}$ to solve the lithium problem with $m_J = 100 \text{ MeV}$ and $m_\phi = 20 \text{ MeV}$. $Y_\phi^{(0)}$ is chosen to satisfy the deuterium constraint at each point. $({}^7\text{Li} + {}^7\text{Be})/\text{H}$ is depicted by gray contours with labels indicating its value, and the shaded gray region solves the lithium problem within 2σ .

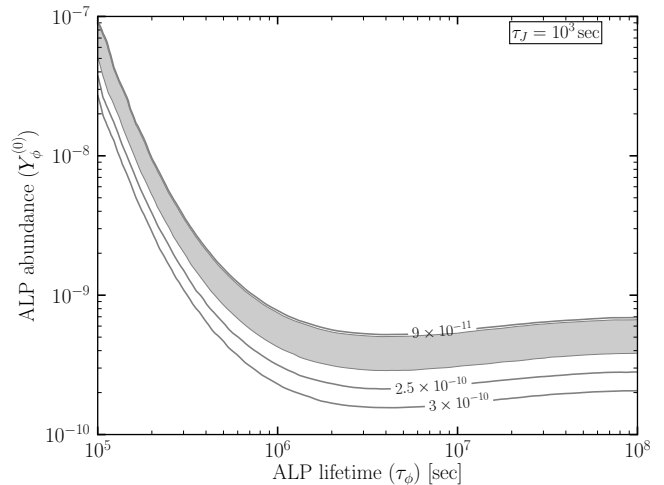


FIG. 9. Working parameter space in $\tau_\phi - Y_\phi^{(0)}$ plane for $\tau_J = 10^3 \text{ sec}$ to solve the lithium problem with $m_J = 100 \text{ MeV}$ and $m_\phi = 20 \text{ MeV}$. $Y_J^{(0)}$ is chosen to satisfy the deuterium constraint at each point. $({}^7\text{Li} + {}^7\text{Be})/\text{H}$ is depicted by gray contours with labels indicating its value, and the shaded gray region solves the lithium problem within 2σ .

ΔN_{eff} constraint from Planck 2018 data [106] and this exclusion becomes stronger if a future experiment such as CMB-S4 [102] can take place.

IV. SUMMARY AND CONCLUSIONS

In this work, we have investigated a bipartite solution to the cosmological lithium problem. Our scenario consists of two distinct stages that work together to reconcile the predicted light-element abundances with ob-

servations. In the first part, neutrinos are injected from the decay of the majoron with its lifetime in the range of $10 \text{ sec} \lesssim \tau_J \lesssim 10^4 \text{ sec}$. The injected neutrinos enhance the $p \rightarrow n$ conversion rate and thus increase the neutron abundance. These excess neutrons successfully decrease the total ${}^7\text{Li} + {}^7\text{Be}$ abundance, but simultaneously lead to an increase in D.

The overproduced deuterium is then addressed in the second part of our scenario. By introducing energetic photons from ALP decay with $\tau_\phi \gtrsim 10^5 \text{ sec}$, the excess D is reduced through photo-dissociation, while the ${}^7\text{Li} + {}^7\text{Be}$

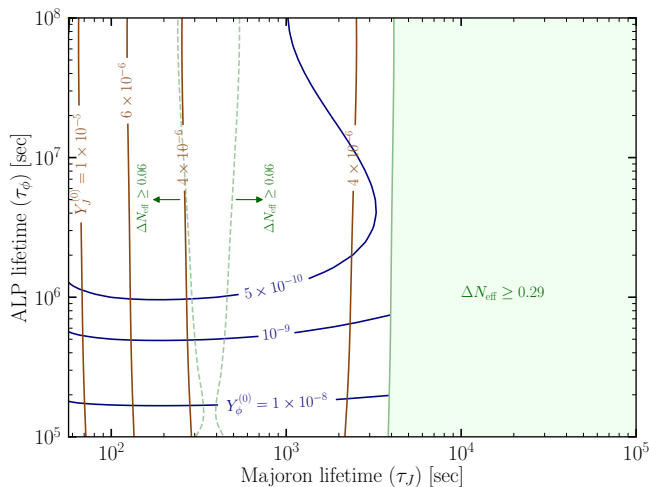


FIG. 10. Parameter space in $\tau_J - \tau_\phi$ plane for solving the lithium problem with $m_J = 100$ MeV and $m_\phi = 20$ MeV. $Y_J^{(0)}$ and $Y_\phi^{(0)}$ are chosen to satisfy the observed central values of D/H and (${}^7\text{Li} + {}^7\text{Be}$)/H at each point. Contours depicted by brown and blue solid lines correspond respectively to $Y_J^{(0)}$ and $Y_\phi^{(0)}$ with labels indicating their values. ΔN_{eff} constraint from Planck 2018 data is shown by the light green shaded region, whereas the light green dashed lines denote future sensitivity expected when the CMB-S4 experiment takes place.

abundance is further decreased. We find that this mechanism can reconcile both lithium and deuterium abundances with the observational data.

It is essential for our scenario that τ_J and τ_ϕ lie in the appropriate ranges, corresponding to the timing of the relevant nuclear and electromagnetic processes. For the majoron to be effective, τ_J should be long enough for substantial ${}^7\text{Be}$ to be converted to ${}^7\text{Li}$ via ${}^7\text{Be}(n, p){}^7\text{Li}$ with the generated extra neutrons, and short enough that the

excess ${}^7\text{Li}$ can still be burned through ${}^7\text{Li}(p, \alpha){}^4\text{He}$. For the ALP to be effective, τ_ϕ should be long enough for the Universe to become sufficiently cooled and transparent to the generated high-energy photons.

This scenario requires an inherent tuning between the two parts in order to reproduce the observed D abundance, which we estimate quantitatively to be of order $\sim 10\%$ in the relation between $Y_\phi^{(0)}$ and $Y_J^{(0)}$. With this requirement, the bipartite approach provides a physically consistent framework for resolving the lithium problem within the main cosmological constraints relevant to this setup.

The parameter region explored in our analysis is therefore not arbitrary, but is guided by the known response of light-element abundances to different decay channels and decay epochs. At the same time, the small initial yields required for a successful bipartite solution are sensitive to the production history of J and ϕ , and may point to nonthermal production or a low reheating temperature rather than a minimal thermal origin. Our setup should therefore be viewed as an explicit proof of concept and as a delineation of viable target regions for future model building, rather than as a complete UV-motivated realization. With this caveat, the present scenario still suggests that, once the deuterium constraint is imposed at its current precision, a viable solution to the lithium problem may require a correlated decay history rather than a single late-time modification.

Acknowledgments

This work was supported by IBS, under the project codes IBS-R018-D1 and IBS-R031-D1. CSS is supported by the National Research Foundation of Korea grant funded by the Korea government RS-2025-25442707 and RS-2026-25498521.

A. PHOTO-DISSOCIATION CROSS SECTIONS OF ${}^7\text{Li}$ AND ${}^7\text{Be}$

In this appendix, we provide the photodissociation cross sections of ${}^7\text{Be}$, ${}^7\text{Li}$, and D. For the processes not discussed here, we adopt the expressions given in Ref. [62], which we find to be consistent with the experimental data. Here the energy of the injected photons in unit of MeV is denoted by \bar{E}_γ . The photodissociation cross-sections are as follows.

1. ${}^7\text{Be}(\gamma, {}^3\text{He}){}^4\text{He}$:

$$\sigma_{\tau_{\text{Be}\gamma \rightarrow {}^3\text{He}{}^4\text{He}}} = \frac{0.5}{1.43} \left(\frac{\mu}{\text{MeV}} \right) \bar{E}_{\text{cm}} \bar{E}_\gamma^{-2} \left(\frac{\exp(-2\pi\eta)}{\bar{E}_{\text{cm}}} \right) \mathcal{G}_1(\bar{E}_{\text{cm}}), \quad (\text{A1})$$

where the threshold energy in unit of MeV (\bar{Q}) = 1.587, $\bar{E}_{\text{cm}} = \bar{E}_\gamma - \bar{Q}$, $2\pi\eta = 5.191/\sqrt{\bar{E}_{\text{cm}}}$, $\mu = 1602.16$ MeV and the functional form of $\mathcal{G}_1(\bar{E}_{\text{cm}})$ is given by

$$\mathcal{G}_1(\bar{E}_{\text{cm}}) = 0.493 \text{ mb} \exp(-0.568\bar{E}_{\text{cm}}) [1 + 0.185\bar{E}_{\text{cm}}^2 + 0.04\bar{E}_{\text{cm}}^3 + 0.015\bar{E}_{\text{cm}}^4]. \quad (\text{A2})$$

2. ${}^7\text{Li}(\gamma, \text{T}){}^4\text{He}$:

$$\sigma_{\tau_{\text{Li}\gamma \rightarrow {}^4\text{HeT}}} = (0.01813 \text{ mb}) e^{-0.5607\bar{E}_\gamma} \times (1 - 18.52\bar{E}_\gamma^2 + 6.748\bar{E}_\gamma^3 + 0.1811\bar{E}_\gamma^4). \quad (\text{A3})$$

$\tau_\phi = 10^5 \text{ sec}$							
$\tau_J \text{ [sec]}$	a_1	b_1	c_1	a_2	b_2	c_2	d_2
10^1	2.52×10^{-5}	0.38	6.64×10^6	4.64×10^{-10}	4.78×10^4	5.43×10^3	1.27×10^6
10^2	2.54×10^{-5}	1.67	6.64×10^6	4.63×10^{-10}	2.04×10^5	1.15×10^4	1.25×10^6
10^3	2.57×10^{-5}	4.60	6.64×10^6	4.59×10^{-10}	4.11×10^5	1.44×10^4	1.21×10^6
10^4	2.53×10^{-5}	2.67	6.64×10^6	4.63×10^{-10}	1.24×10^5	1.22×10^4	1.16×10^6
10^5	2.52×10^{-5}	0.52	6.64×10^6	4.64×10^{-10}	1.90×10^4	2.38×10^3	1.22×10^6
$\tau_\phi = 3.98 \times 10^5 \text{ sec}$							
10^1	2.52×10^{-5}	0.38	2.77×10^8	4.64×10^{-10}	4.78×10^4	5.44×10^3	6.61×10^7
10^2	2.54×10^{-5}	1.67	2.77×10^8	4.63×10^{-10}	2.04×10^5	1.15×10^4	6.59×10^7
10^3	2.57×10^{-5}	4.60	2.77×10^8	4.59×10^{-10}	4.10×10^5	1.45×10^4	6.53×10^7
10^4	2.53×10^{-5}	2.67	2.77×10^8	4.62×10^{-10}	1.22×10^5	1.21×10^4	6.45×10^7
10^5	2.52×10^{-5}	0.52	2.77×10^8	4.64×10^{-10}	1.86×10^4	2.21×10^3	6.55×10^7
$\tau_\phi = 1.58 \times 10^6 \text{ sec}$							
10^1	2.52×10^{-5}	0.38	9.66×10^8	4.64×10^{-10}	4.78×10^4	5.42×10^3	2.51×10^8
10^2	2.54×10^{-5}	1.67	9.66×10^8	4.63×10^{-10}	2.04×10^5	1.14×10^4	2.50×10^8
10^3	2.57×10^{-5}	4.60	9.66×10^8	4.60×10^{-10}	4.12×10^5	1.43×10^4	2.50×10^8
10^4	2.53×10^{-5}	2.67	9.66×10^8	4.64×10^{-10}	1.25×10^5	1.22×10^4	2.49×10^8
10^5	2.52×10^{-5}	0.52	9.66×10^8	4.64×10^{-10}	1.92×10^4	2.47×10^3	2.50×10^8
$\tau_\phi = 6.31 \times 10^6 \text{ sec}$							
10^1	2.52×10^{-5}	0.38	1.13×10^9	4.64×10^{-10}	4.79×10^4	5.37×10^3	3.20×10^8
10^2	2.54×10^{-5}	1.67	1.13×10^9	4.63×10^{-10}	2.05×10^5	1.12×10^4	3.21×10^8
10^3	2.57×10^{-5}	4.60	1.13×10^9	4.61×10^{-10}	4.17×10^5	1.39×10^4	3.24×10^8
10^4	2.53×10^{-5}	2.67	1.13×10^9	4.66×10^{-10}	1.29×10^5	1.24×10^4	3.27×10^8
10^5	2.52×10^{-5}	0.52	1.13×10^9	4.65×10^{-10}	2.09×10^4	3.08×10^3	3.23×10^8
$\tau_\phi = 2.51 \times 10^7 \text{ sec}$							
10^1	2.52×10^{-5}	0.38	9.25×10^8	4.64×10^{-10}	4.81×10^4	5.33×10^3	2.82×10^8
10^2	2.54×10^{-5}	1.67	9.25×10^8	4.63×10^{-10}	2.06×10^5	1.10×10^4	2.84×10^8
10^3	2.57×10^{-5}	4.60	9.25×10^8	4.62×10^{-10}	4.21×10^5	1.35×10^4	2.89×10^8
10^4	2.53×10^{-5}	2.67	9.25×10^8	4.68×10^{-10}	1.34×10^5	1.26×10^4	2.95×10^8
10^5	2.52×10^{-5}	0.52	9.25×10^8	4.66×10^{-10}	2.25×10^4	3.58×10^3	2.87×10^8
$\tau_\phi = 10^8 \text{ sec}$							
10^1	2.52×10^{-5}	0.38	8.47×10^8	4.64×10^{-10}	4.81×10^4	5.31×10^3	2.64×10^8
10^2	2.54×10^{-5}	1.67	8.47×10^8	4.63×10^{-10}	2.06×10^5	1.09×10^4	2.66×10^8
10^3	2.57×10^{-5}	4.60	8.47×10^8	4.62×10^{-10}	4.23×10^5	1.33×10^4	2.72×10^8
10^4	2.53×10^{-5}	2.67	8.47×10^8	4.68×10^{-10}	1.36×10^5	1.26×10^4	2.79×10^8
10^5	2.52×10^{-5}	0.52	8.47×10^8	4.66×10^{-10}	2.31×10^4	3.75×10^3	2.70×10^8

TABLE I. Fitting coefficients for $m_J = 100 \text{ MeV}$, and $m_\phi = 20 \text{ MeV}$.

where $\bar{Q} = 2.46703$ is the threshold energy of the reaction, in units of MeV.

3. ${}^7\text{Li}(\gamma, n){}^6\text{Li}$:

$$\sigma_{\tau\text{Li}\gamma \rightarrow n{}^6\text{Li}} = 0.176 \text{ mb } \bar{Q}^{1.51} \bar{E}_{\text{cm}}^{0.49} \bar{E}_\gamma^{-2} + 1205 \text{ mb } \bar{Q}^{5.5} \bar{E}_{\text{cm}}^5 \bar{E}_\gamma^{-10.5} + 0.06 \text{ mb } \left[1 + \left(\frac{\bar{E}_{\text{cm}} - 7.46}{0.188} \right)^2 \right]^{-1}, \quad (\text{A4})$$

where $\bar{Q} = 7.25$, and $\bar{E}_{\text{cm}} = \bar{E}_\gamma - \bar{Q}$.

4. ${}^7\text{Li}(\gamma, 2np){}^4\text{He}$:

$$\sigma_{\tau\text{Li}\gamma \rightarrow 2np{}^4\text{He}} = 122 \text{ mb } \frac{\bar{Q}^4 \bar{E}_{\text{cm}}^3}{\bar{E}_\gamma^7}, \quad (\text{A5})$$

where $\bar{Q} = 10.95 \text{ MeV}$, and $\bar{E}_{\text{cm}} = \bar{E}_\gamma - \bar{Q}$.

B. FITTING COEFFICIENTS

The fitting coefficients in Eq. (20), and (21) are given in Tab. I.

-
- [1] R. V. Wagoner, W. A. Fowler, and F. Hoyle, On the Synthesis of elements at very high temperatures, *Astrophys. J.* **148**, 3 (1967).
- [2] F. Spite and M. Spite, Abundance of lithium in unevolved halo stars and old disk stars: Interpretation and consequences, *Astron. Astrophys.* **115**, 357 (1982).
- [3] C. Pitrou, A. Coc, J.-P. Uzan, and E. Vangioni, Precision big bang nucleosynthesis with improved Helium-4 predictions, *Phys. Rept.* **754**, 1 (2018), arXiv:1801.08023 [astro-ph.CO].
- [4] C. Pitrou, A. Coc, J.-P. Uzan, and E. Vangioni, A new tension in the cosmological model from primordial deuterium?, *Mon. Not. Roy. Astron. Soc.* **502**, 2474 (2021), arXiv:2011.11320 [astro-ph.CO].
- [5] T.-H. Yeh, J. Shelton, K. A. Olive, and B. D. Fields, Probing physics beyond the standard model: limits from BBN and the CMB independently and combined, *JCAP* **10**, 046, arXiv:2207.13133 [astro-ph.CO].
- [6] O. Pisanti, A. Cirillo, S. Esposito, F. Iocco, G. Mangano, G. Miele, and P. D. Serpico, PArthENoPE: Public Algorithm Evaluating the Nucleosynthesis of Primordial Elements, *Comput. Phys. Commun.* **178**, 956 (2008), arXiv:0705.0290 [astro-ph].
- [7] S. Gariazzo, P. F. de Salas, O. Pisanti, and R. Consiglio, PArthENoPE revolutions, *Comput. Phys. Commun.* **271**, 108205 (2022), arXiv:2103.05027 [astro-ph.IM].
- [8] A.-K. Burns, T. M. P. Tait, and M. Valli, PRyMordial: the first three minutes, within and beyond the standard model, *Eur. Phys. J. C* **84**, 86 (2024), arXiv:2307.07061 [hep-ph].
- [9] A. Pinto *et al.*, The metal-poor end of the Spite plateau II. Chemical and dynamical investigation, *Astron. Astrophys.* **654**, A170 (2021).
- [10] S. Navas *et al.* (Particle Data Group), Review of particle physics, *Phys. Rev. D* **110**, 030001 (2024), and 2025 update.
- [11] G. Michaud, G. Fontaine, and G. Beaudet, The lithium abundance - Constraints on stellar evolution, *Astrophys. J.* **282**, 206 (1984).
- [12] S. Vauclair, Lithium Nuclear Destruction in Stellar Outer Layers: A Consistent Theoretical View of the Characteristic Features Observed in Young and Old Stars, *Astrophys. J.* **335**, 971 (1988).
- [13] C. R. Proffitt and G. Michaud, Diffusion and Mixing of Lithium and Helium in Population II Dwarfs, *Astrophys. J.* **371**, 584 (1991).
- [14] B. Chaboyer and P. Demarque, ^7Li Abundances in Halo Stars: Testing Stellar Evolution Models and the Primordial ^7Li Abundance, *Astrophys. J.* **433**, 510 (1994), arXiv:astro-ph/9403043 [astro-ph].
- [15] S. Vauclair and C. Charbonnel, Influence of a stellar wind on the lithium depletion in halo stars: a new step towards the lithium primordial abundance, *Astron. Astrophys.* **295**, 715 (1995).
- [16] S. Vauclair and C. Charbonnel, Element Segregation in Low-Metallicity Stars and the Primordial Lithium Abundance, *Astrophys. J.* **502**, 372 (1998), arXiv:astro-ph/9802315 [astro-ph].
- [17] M. Salaris and A. Weiss, Atomic diffusion in metal-poor stars. II. Predictions for the Spite plateau (2001), arXiv:astro-ph/0104406 [astro-ph].
- [18] O. Richard, G. Michaud, J. Richer, S. Turcotte, S. Turck-Chieze, and D. A. Vandenberg, Models of metal poor stars with gravitational settling and radiative accelerations: I. evolution and abundance anomalies, *Astrophys. J.* **580**, 1100 (2002), arXiv:astro-ph/0112113.
- [19] O. Richard, G. Michaud, J. Richer, S. Turcotte, S. Turck-Chieze, and D. A. Vandenberg, Models of metal poor stars with gravitational settling and radiative accelerations: I. evolution and abundance anomalies, *Astrophys. J.* **580**, 1100 (2002), arXiv:astro-ph/0112113.
- [20] O. Richard, G. Michaud, and J. Richer, Implications of WMAP observations on Li abundance and stellar evolution models, *Astrophys. J.* **619**, 538 (2005), arXiv:astro-ph/0409672.
- [21] L. Piau, T. C. Beers, D. S. Balsara, T. Sivarani, J. W. Truran, and J. W. Ferguson, From First Stars to the Spite Plateau: a Possible Reconciliation of Halo Stars Observations with Predictions from Big Bang Nucleosynthesis, *Astrophys. J.* **653**, 300 (2006), arXiv:astro-ph/0603553.
- [22] A. J. Korn, F. Grundahl, O. Richard, P. S. Barklem, L. Mashonkina, R. Collet, N. Piskunov, and B. Gustafsson, A probable stellar solution to the cosmological lithium discrepancy, *Nature* **442**, 657 (2006), arXiv:astro-ph/0608201.
- [23] L. Piau, Lithium Isotopes in Population II Dwarfs, *Astrophys. J.* **689**, 1279 (2008).
- [24] M. Vick, G. Michaud, J. Richer, and O. Richard, Population II stars and the Spite plateau; Stellar evolution models with mass loss, *Astron. Astrophys.* **552**, A131 (2013), arXiv:1304.0815 [astro-ph.SR].
- [25] X. Fu, A. Bressan, P. Molaro, and P. Marigo, Lithium evolution in metal-poor stars: from pre-main sequence to the Spite plateau, *Mon. Not. Roy. Astron. Soc.* **452**, 3256 (2015), arXiv:1506.05993 [astro-ph.SR].
- [26] V. Grisoni, F. Matteucci, D. Romano, and X. Fu, Evolution of lithium in the Milky Way halo, discs, and bulge, *Mon. Not. Roy. Astron. Soc.* **489**, 3539 (2019), arXiv:1906.09130 [astro-ph.GA].
- [27] M. Deal, M.-J. Goupil, J. Marques, D. Reese, and Y. Lebreton, Chemical mixing in low mass stars. I. Rotation against atomic diffusion including radiative acceleration, *Astron. Astrophys.* **633**, A23 (2020), arXiv:1910.14335 [astro-ph.SR].
- [28] E. Tognelli, P. G. Prada Moroni, S. Degl'Innocenti, M. Salaris, and S. Cassisi, Protostellar accretion in low mass metal poor stars and the cosmological lithium problem, *Astron. Astrophys.* **638**, A81 (2020), arXiv:2004.14857 [astro-ph.SR].
- [29] T. Dumont, C. Charbonnel, A. Palacios, and S. Borisov, Lithium depletion and angular momentum transport in F-type and G-type stars in Galactic open clusters, *Astron. Astrophys.* **654**, A46 (2021), arXiv:2107.12060 [astro-ph.SR].
- [30] T. Dumont, A. Palacios, C. Charbonnel, O. Richard, L. Amard, K. Augustson, and S. Mathis, Lithium depletion and angular momentum transport in solar-type stars, *Astron. Astrophys.* **646**, A48 (2021), arXiv:2012.03647 [astro-ph.SR].

- [31] S. Borisov, C. Charbonnel, N. Prantzos, T. Dumont, and A. Palacios, A coherent view of Li depletion and angular momentum transport to explain the Li plateau – from Population II to Population I stars, *Astron. Astrophys.* **690**, A245 (2025), arXiv:2403.15534 [astro-ph.SR].
- [32] A. Korn, The ups and downs of inferred cosmological lithium, *EPJ Web Conf.* **297**, 01007 (2024), arXiv:2406.09974 [astro-ph.SR].
- [33] E. X. Wang, T. Nordlander, M. Asplund, K. Lind, Y. Zhou, and H. Reggiani, Non-detection of ${}^6\text{Li}$ in Spite plateau stars with ESPRESSO, *Mon. Not. Roy. Astron. Soc.* **509**, 1521 (2022), arXiv:2110.03822 [astro-ph.SR].
- [34] B. D. Fields and K. A. Olive, Implications of the non-observation of ${}^6\text{Li}$ in halo stars for the primordial ${}^7\text{Li}$ problem, *JCAP* **10**, 078, arXiv:2204.03167 [astro-ph.GA].
- [35] M. H. Reno and D. Seckel, Primordial Nucleosynthesis: The Effects of Injecting Hadrons, *Phys. Rev. D* **37**, 3441 (1988).
- [36] K. Jedamzik, Did something decay, evaporate, or annihilate during Big Bang nucleosynthesis?, *Phys. Rev. D* **70**, 063524 (2004), arXiv:astro-ph/0402344.
- [37] M. Pospelov and J. Pradler, Metastable GeV-scale particles as a solution to the cosmological lithium problem, *Phys. Rev. D* **82**, 103514 (2010), arXiv:1006.4172 [hep-ph].
- [38] D. Albornoz Vasquez, A. Belikov, A. Coc, J. Silk, and E. Vangioni, Neutron injection during primordial nucleosynthesis alleviates the primordial ${}^7\text{Li}$ problem, *Phys. Rev. D* **86**, 063501 (2012), arXiv:1208.0443 [astro-ph.CO].
- [39] A. Coc, M. Pospelov, J.-P. Uzan, and E. Vangioni, Modified big bang nucleosynthesis with nonstandard neutron sources, *Phys. Rev. D* **90**, 085018 (2014), arXiv:1405.1718 [hep-ph].
- [40] M. Kusakabe, M.-K. Cheoun, and K. S. Kim, General limit on the relation between abundances of D and ${}^7\text{Li}$ in big bang nucleosynthesis with nucleon injections, *Phys. Rev. D* **90**, 045009 (2014), arXiv:1404.3090 [astro-ph.CO].
- [41] M. Kawasaki, K. Kohri, T. Moroi, and Y. Takaesu, Revisiting Big-Bang Nucleosynthesis Constraints on Long-Lived Decaying Particles, *Phys. Rev. D* **97**, 023502 (2018), arXiv:1709.01211 [hep-ph].
- [42] M. Kusakabe, A. B. Balantekin, T. Kajino, and Y. Pehlivan, Big-bang nucleosynthesis limit on the neutral fermion decays into neutrinos, *Phys. Rev. D* **87**, 085045 (2013), arXiv:1303.2291 [astro-ph.CO].
- [43] L. Salvati, L. Pagano, M. Lattanzi, M. Gerbino, and A. Melchiorri, Breaking Be: a sterile neutrino solution to the cosmological lithium problem, *JCAP* **08**, 022, arXiv:1606.06968 [astro-ph.CO].
- [44] S. Chang, S. Ganguly, T. H. Jung, T.-S. Park, and C. S. Shin, Constraining MeV to 10 GeV Majorons by big bang nucleosynthesis, *Phys. Rev. D* **110**, 015019 (2024), arXiv:2401.00687 [hep-ph].
- [45] A. Goudelis, M. Pospelov, and J. Pradler, Light Particle Solution to the Cosmic Lithium Problem, *Phys. Rev. Lett.* **116**, 211303 (2016), arXiv:1510.08858 [hep-ph].
- [46] O. Erken, P. Sikivie, H. Tam, and Q. Yang, Axion Dark Matter and Cosmological Parameters, *Phys. Rev. Lett.* **108**, 061304 (2012), arXiv:1104.4507 [astro-ph.CO].
- [47] M. Kusakabe, A. B. Balantekin, T. Kajino, and Y. Pehlivan, Solution to Big-Bang Nucleosynthesis in Hybrid Axion Dark Matter Model, *Phys. Lett. B* **718**, 704 (2013), arXiv:1202.5603 [astro-ph.CO].
- [48] M. Kawasaki, K. Kohri, T. Moroi, K. Murai, and H. Murayama, Big-bang nucleosynthesis with sub-GeV massive decaying particles, *JCAP* **12**, 048, arXiv:2006.14803 [hep-ph].
- [49] Y. Luo, T. Kajino, M. Kusakabe, and G. J. Mathews, Big Bang Nucleosynthesis with an Inhomogeneous Primordial Magnetic Field Strength, *Astrophys. J.* **872**, 172 (2019), arXiv:1810.08803 [astro-ph.CO].
- [50] N. Yamanaka, Light nuclei under magnetic field and the lithium problem, (2025), arXiv:2509.03684 [nucl-th].
- [51] S. Koren, Cosmological Lithium Solution from Discrete Gauged B-L, *Phys. Rev. Lett.* **131**, 091003 (2023), arXiv:2204.01750 [hep-ph].
- [52] R. Cooke, M. Pettini, R. A. Jorgenson, M. T. Murphy, and C. C. Steidel, Precision measures of the primordial abundance of deuterium, *Astrophys. J.* **781**, 31 (2014), arXiv:1308.3240 [astro-ph.CO].
- [53] R. J. Cooke, M. Pettini, K. M. Nollett, and R. Jorgenson, The primordial deuterium abundance of the most metal-poor damped Ly α system, *Astrophys. J.* **830**, 148 (2016), arXiv:1607.03900 [astro-ph.CO].
- [54] S. Riemer-Sørensen, J. K. Webb, N. Crighton, V. Dumont, K. Ali, S. Kotuš, M. Bainbridge, M. T. Murphy, and R. Carswell, A robust deuterium abundance; Re-measurement of the $z=3.256$ absorption system towards the quasar PKS1937-1009, *Mon. Not. Roy. Astron. Soc.* **447**, 2925 (2015), arXiv:1412.4043 [astro-ph.CO].
- [55] S. A. Balashev, E. O. Zavarygin, A. V. Ivanchik, K. N. Telikova, and D. A. Varshalovich, The primordial deuterium abundance: subDLA system at $z_{\text{abs}} = 2.437$ towards the QSO J 1444+2919, *Mon. Not. Roy. Astron. Soc.* **458**, 2188 (2016), arXiv:1511.01797 [astro-ph.GA].
- [56] S. Riemer-Sørensen, S. Kotuš, J. K. Webb, K. Ali, V. Dumont, M. T. Murphy, and R. F. Carswell, A precise deuterium abundance: remeasurement of the $z = 3.572$ absorption system towards the quasar PKS1937-101, *Mon. Not. Roy. Astron. Soc.* **468**, 3239 (2017), arXiv:1703.06656 [astro-ph.CO].
- [57] E. O. Zavarygin, J. K. Webb, V. Dumont, and S. Riemer-Sørensen, The primordial deuterium abundance at $z_{\text{abs}} = 2.504$ from a high signal-to-noise spectrum of Q1009+2956, *Mon. Not. Roy. Astron. Soc.* **477**, 5536 (2018), arXiv:1706.09512 [astro-ph.GA].
- [58] R. J. Cooke, M. Pettini, and C. C. Steidel, One Percent Determination of the Primordial Deuterium Abundance, *Astrophys. J.* **855**, 102 (2018), arXiv:1710.11129 [astro-ph.CO].
- [59] T.-H. Yeh, K. A. Olive, and B. D. Fields, The impact of new $d(p, \gamma)3$ rates on Big Bang Nucleosynthesis, *JCAP* **03**, 046, arXiv:2011.13874 [astro-ph.CO].
- [60] M. Kawasaki and T. Moroi, Electromagnetic cascade in the early universe and its application to the big bang nucleosynthesis, *Astrophys. J.* **452**, 506 (1995), arXiv:astro-ph/9412055.
- [61] M. Hufnagel, K. Schmidt-Hoberg, and S. Wild, BBN constraints on MeV-scale dark sectors. Part II. Electromagnetic decays, *JCAP* **11**, 032, arXiv:1808.09324 [hep-ph].
- [62] R. H. Cyburt, J. R. Ellis, B. D. Fields, and K. A. Olive, Updated nucleosynthesis constraints on unstable relic particles, *Phys. Rev. D* **67**, 103521 (2003), arXiv:astro-

- ph/0211258.
- [63] R. J. Scherrer, Deuterium and helium-3 production from massive neutrino decay, *Mon. Not. Roy. Astron. Soc.* **210**, 359 (1984).
- [64] S. Chang and K. Choi, Constraints from nucleosynthesis and SN1987A on majoron emitting double beta decay, *Phys. Rev. D* **49**, 12 (1994), arXiv:hep-ph/9303243.
- [65] T. Kanzaki, M. Kawasaki, K. Kohri, and T. Moroi, Cosmological Constraints on Neutrino Injection, *Phys. Rev. D* **76**, 105017 (2007), arXiv:0705.1200 [hep-ph].
- [66] S. Bianco, P. F. Depta, J. Frerick, T. Hambye, M. Hufnagel, and K. Schmidt-Hoberg, Photo- and hadrodissintegration constraints on massive relics decaying into neutrinos, *JCAP* **11**, 072, arXiv:2505.01492 [hep-ph].
- [67] R. J. Scherrer and M. S. Turner, Primordial Nucleosynthesis with Decaying Particles: 1. Entropy Producing Decays, 2. Inert Decays, *Astrophys. J.* **331**, 19 (1988).
- [68] S. Sarkar and A. M. Cooper-Sarkar, Cosmological and experimental constraints on the tau neutrino, *Phys. Lett. B* **148**, 347 (1984).
- [69] J. R. Ellis, D. V. Nanopoulos, and S. Sarkar, The Cosmology of Decaying Gravitinos, *Nucl. Phys. B* **259**, 175 (1985).
- [70] R. J. Protheroe, T. Stanev, and V. S. Berezhinsky, Electromagnetic cascades and cascade nucleosynthesis in the early universe, *Phys. Rev. D* **51**, 4134 (1995), arXiv:astro-ph/9409004.
- [71] E. Holtmann, M. Kawasaki, K. Kohri, and T. Moroi, Radiative decay of a longlived particle and big bang nucleosynthesis, *Phys. Rev. D* **60**, 023506 (1999), arXiv:hep-ph/9805405.
- [72] M. Kawasaki, K. Kohri, and T. Moroi, Radiative decay of a massive particle and the nonthermal process in primordial nucleosynthesis, *Phys. Rev. D* **63**, 103502 (2001), arXiv:hep-ph/0012279.
- [73] K. Jedamzik, Big bang nucleosynthesis constraints on hadronically and electromagnetically decaying relic neutral particles, *Phys. Rev. D* **74**, 103509 (2006), arXiv:hep-ph/0604251.
- [74] V. Poulin and P. D. Serpico, Loophole to the Universal Photon Spectrum in Electromagnetic Cascades and Application to the Cosmological Lithium Problem, *Phys. Rev. Lett.* **114**, 091101 (2015), arXiv:1502.01250 [astro-ph.CO].
- [75] V. Poulin and P. D. Serpico, Nonuniversal BBN bounds on electromagnetically decaying particles, *Phys. Rev. D* **91**, 103007 (2015), arXiv:1503.04852 [astro-ph.CO].
- [76] L. Forestell, D. E. Morrissey, and G. White, Limits from BBN on Light Electromagnetic Decays, *JHEP* **01**, 074, arXiv:1809.01179 [hep-ph].
- [77] K. Kohri and J. Yokoyama, Primordial black holes and primordial nucleosynthesis. 1. Effects of hadron injection from low mass holes, *Phys. Rev. D* **61**, 023501 (2000), arXiv:astro-ph/9908160.
- [78] M. Kawasaki, K. Kohri, and N. Sugiyama, MeV scale reheating temperature and thermalization of neutrino background, *Phys. Rev. D* **62**, 023506 (2000), arXiv:astro-ph/0002127.
- [79] K. Kohri, Primordial nucleosynthesis and hadronic decay of a massive particle with a relatively short lifetime, *Phys. Rev. D* **64**, 043515 (2001), arXiv:astro-ph/0103411.
- [80] M. Kawasaki, K. Kohri, and T. Moroi, Big-Bang nucleosynthesis and hadronic decay of long-lived massive particles, *Phys. Rev. D* **71**, 083502 (2005), arXiv:astro-ph/0408426.
- [81] M. Kawasaki, K. Kohri, and T. Moroi, Hadronic decay of the gravitino in the early universe and its implications to inflation, in *10th International Symposium on Particles, Strings and Cosmology (PASCOS 04 and Prana Nath Fest)* (2004) pp. 411–416, arXiv:hep-ph/0410287.
- [82] M. Kawasaki, K. Kohri, and T. Moroi, Hadronic decay of late - decaying particles and Big-Bang Nucleosynthesis, *Phys. Lett. B* **625**, 7 (2005), arXiv:astro-ph/0402490.
- [83] K. Kohri, T. Moroi, and A. Yotsuyanagi, Big-bang nucleosynthesis with unstable gravitino and upper bound on the reheating temperature, *Phys. Rev. D* **73**, 123511 (2006), arXiv:hep-ph/0507245.
- [84] M. Kawasaki, K. Kohri, T. Moroi, and A. Yotsuyanagi, Big-Bang Nucleosynthesis and Gravitino, *Phys. Rev. D* **78**, 065011 (2008), arXiv:0804.3745 [hep-ph].
- [85] R. H. Cyburt, J. Ellis, B. D. Fields, F. Luo, K. A. Olive, and V. C. Spanos, Nucleosynthesis Constraints on a Massive Gravitino in Neutralino Dark Matter Scenarios, *JCAP* **10**, 021, arXiv:0907.5003 [astro-ph.CO].
- [86] K. Jedamzik and M. Pospelov, Big Bang Nucleosynthesis and Particle Dark Matter, *New J. Phys.* **11**, 105028 (2009), arXiv:0906.2087 [hep-ph].
- [87] R. H. Cyburt, J. Ellis, B. D. Fields, F. Luo, K. A. Olive, and V. C. Spanos, Nuclear Reaction Uncertainties, Massive Gravitino Decays and the Cosmological Lithium Problem, *JCAP* **10**, 032, arXiv:1007.4173 [astro-ph.CO].
- [88] B. Henning and H. Murayama, Constraints on Light Dark Matter from Big Bang Nucleosynthesis, (2012), arXiv:1205.6479 [hep-ph].
- [89] A. Fradette, M. Pospelov, J. Pradler, and A. Ritz, Cosmological Constraints on Very Dark Photons, *Phys. Rev. D* **90**, 035022 (2014), arXiv:1407.0993 [hep-ph].
- [90] J. Berger, K. Jedamzik, and D. G. E. Walker, Cosmological Constraints on Decoupled Dark Photons and Dark Higgs, *JCAP* **11**, 032, arXiv:1605.07195 [hep-ph].
- [91] A. Fradette and M. Pospelov, BBN for the LHC: constraints on lifetimes of the Higgs portal scalars, *Phys. Rev. D* **96**, 075033 (2017), arXiv:1706.01920 [hep-ph].
- [92] T. Hasegawa, N. Hiroshima, K. Kohri, R. S. L. Hansen, T. Tram, and S. Hannestad, MeV-scale reheating temperature and thermalization of oscillating neutrinos by radiative and hadronic decays of massive particles, *JCAP* **12**, 012, arXiv:1908.10189 [hep-ph].
- [93] A. Boyarsky, M. Ovchinnikov, O. Ruchayskiy, and V. Syvolap, Improved big bang nucleosynthesis constraints on heavy neutral leptons, *Phys. Rev. D* **104**, 023517 (2021), arXiv:2008.00749 [hep-ph].
- [94] Y.-M. Chen and Y. Zhang, BBN constraint on heavy neutrino production and decay, *Phys. Rev. D* **111**, 123024 (2025), arXiv:2410.07343 [hep-ph].
- [95] A. Omar and A. Ritz, BBN constraints on the hadronic annihilation of sub-GeV dark matter, *Phys. Rev. D* **113**, 035004 (2026), arXiv:2510.11791 [hep-ph].
- [96] L. Angel, G. Arcadi, M. M. A. Paixão, and F. S. Queiroz, Updated BBN Bounds on Hadronic Injection in the Early Universe: The Gravitino Problem, (2025), arXiv:2501.09120 [hep-ph].
- [97] T. H. Jung, T. Okui, K. Tobioka, and J. Wang, New bounds on heavy QCD axions from big bang nucleosynthesis, *Phys. Rev. D* **113**, 055002 (2026),

- arXiv:2510.23695 [hep-ph].
- [98] G. Mangano, G. Miele, S. Pastor, and M. Peloso, A Precision calculation of the effective number of cosmological neutrinos, *Phys. Lett. B* **534**, 8 (2002), arXiv:astro-ph/0111408.
- [99] G. Mangano, G. Miele, S. Pastor, T. Pinto, O. Pisanti, and P. D. Serpico, Relic neutrino decoupling including flavor oscillations, *Nucl. Phys. B* **729**, 221 (2005), arXiv:hep-ph/0506164.
- [100] G. Mangano, G. Miele, S. Pastor, T. Pinto, O. Pisanti, and P. D. Serpico, Effects of non-standard neutrino-electron interactions on relic neutrino decoupling, *Nucl. Phys. B* **756**, 100 (2006), arXiv:hep-ph/0607267.
- [101] D. F. G. Fiorillo, G. G. Raffelt, and E. Vitagliano, Strong Supernova 1987A Constraints on Bosons Decaying to Neutrinos, *Phys. Rev. Lett.* **131**, 021001 (2023), arXiv:2209.11773 [hep-ph].
- [102] K. N. Abazajian *et al.* (CMB-S4), *CMB-S4 Science Book, First Edition* (2016) arXiv:1610.02743 [astro-ph.CO].
- [103] D. S. Balsaer and T. M. Bania, Green Bank Telescope Observations of $^3\text{He}^+$: H II Regions, *The Astronomical Journal* **156**, 280 (2018), arXiv:1810.09422 [astro-ph.GA].
- [104] R. J. Cooke, P. Noterdaeme, J. W. Johnson, M. Pettini, L. Welsh, C. Peroux, M. T. Murphy, and D. H. Weinberg, Primordial Helium-3 Redux: The Helium Isotope Ratio of the Orion Nebula, *Astrophys. J.* **932**, 60 (2022), arXiv:2203.11256 [astro-ph.CO].
- [105] N. Iwamoto, K. Kosako, and T. Fukahori, JENDL photonuclear data file 2016, *Journal of Nuclear Science and Technology* **60**, 911 (2023).
- [106] N. Aghanim *et al.* (Planck), Planck 2018 results. VI. Cosmological parameters, *Astron. Astrophys.* **641**, A6 (2020), [Erratum: *Astron. Astrophys.* 652, C4 (2021)], arXiv:1807.06209 [astro-ph.CO].